You might find this additional information useful...

This article cites 33 articles, 20 of which you can access free at:
http://ajprenal.physiology.org/cgi/content/full/296/5/F1023#BIBL

Updated information and services including high-resolution figures, can be found at:
http://ajprenal.physiology.org/cgi/content/full/296/5/F1023

Additional material and information about *AJP - Renal Physiology* can be found at:
http://www.the-aps.org/publications/ajprenal

This information is current as of April 26, 2009 .

Contrast angiography of the rat renal microcirculation in vivo using synchrotron radiation

Gabriela A. Eppel,[1] David Lo Jacono,[2] Mikiyasu Shirai,[3] Keiji Umetani,[4] Roger G. Evans,[1] and James T. Pearson[1,5]

Departments of [1]Physiology and [2]Mechanical and Aerospace Engineering, Monash University, Melbourne, Australia; [3]Department of Clinical Radiology, Hiroshima International University, Hiroshima; [4]Japan Synchrotron Radiation Research Institute, Hyogo, Japan; and [5]Monash Centre for Synchrotron Science, Monash University, Melbourne, Australia

Eppel GA, Jacono DL, Shirai M, Umetani K, Evans RG, Pearson JT. Contrast angiography of the rat renal microcirculation in vivo using synchrotron radiation. *Am J Physiol Renal Physiol* 296: F1023–F1031, 2009. First published March 4, 2009; doi:10.1152/ajprenal.90499.2008.—We have developed a new method for contrast microangiography of the rat renal circulation using synchrotron radiation. The method was applied to determine responses of the renal arterial vasculature to angiotensin II and electrical stimulation of the renal nerves (RNS). Iodinated contrast agent was administered directly into the renal artery of pentobarbital-anesthetized rats before and during *1*) intravenous infusion of angiotensin II (1.6 $\mu g \cdot kg^{-1} \cdot min^{-1}$) or *2*) its vehicle, or *3*) RNS at 2 Hz. Images were obtained at 30 Hz, before and during these treatments, and vascular caliber was determined by use of a newly developed algorithm described herein. Up to four levels of branching could be observed simultaneously along the arterial tree, comprising vessels with resting diameter of 28–400 μm. Vessel diameter was not significantly altered by vehicle infusion ($+3.1 \pm 3.5\%$ change) but was significantly reduced by angiotensin II ($-24.3 \pm 3.4\%$) and RNS ($-17.1 \pm 3.8\%$). Angiotensin II-induced vasoconstriction was independent of vessel size, but RNS-induced vasoconstriction was greatest in vessels with a resting caliber of 100–200 μm and least in vessels with a resting caliber 40–100 μm. In conclusion, the method we describe herein provides a new approach for assessing responses of the renal arterial circulation to vasoactive factors along several orders of branching.

angiography; angiotensin II; vascular caliber; kidney circulation; renal nerves

RENAL VASCULAR TONE IS A CRITICAL controller of renal perfusion, glomerular filtration rate, and tubular function (21) and thus long-term regulation of body fluid homeostasis (9). Many available methodologies allow quantification of changes in the caliber of resistance vessels in vivo, but all have important limitations. For example, vascular casting techniques allow quantification of vascular caliber at multiple points along the renal vascular tree, potentially allowing analysis of regulation of blood flow within networks of blood vessels in the kidney (4, 5). But an important disadvantage of this approach is that measurements can only be made at a single time point so that the effects of vasoactive factors can only be inferred from cross-sectional comparisons between blood vessels in different animals. Real-time analysis of vascular caliber (17) and capillary blood velocity (33) within the kidney has been achieved with intravital microscopy, but currently the measurements derived from such techniques are limited to single points along

an identified blood vessel. Magnetic resonance imaging and X-ray microtomographic techniques currently lack the spatial and/or temporal resolution required for real-time analysis of resistance vessel caliber in the kidney in vivo (1).

Herein we present a new approach that overcomes some of the limitations of other methods. We have used a high-resolution microimaging system at the Japan Synchrotron Radiation Research Institute (SPring-8, BL28B2 beamline) to obtain contrast angiograms of regions of the renal cortical arterial tree of anesthetized rats. The advantages of the present technique are that *1*) data can be collected in vivo, *2*) measurements of vascular caliber can be repeated within 20 to 30 min, allowing within-animal comparisons of vascular lumen dimensions, and *3*) images are recorded within a 4- to 7-mm window, allowing simultaneous observations of up to four levels of branching of arteries/arterioles from ~30 to 400 μm in diameter. We were able to use the new approach to characterize renal microvascular responses to intravenous infusion of angiotensin II and to electrical stimulation of the renal nerves across a range of different-sized vessels. Currently this technique does not have the required resolution for quantification of afferent and efferent arteriolar caliber. However, this will be possible with development of more radiopaque contrast agents and ultra-high resolution X-ray camera systems. Our present work provides proof of concept for a new method for analysis of segmental vascular function in vivo.

METHODS

Surgical preparation. All experiments were conducted with ethical approval from the SPring-8 Review Committee and the Monash University School of Biomedical Sciences Animal Ethics Committee. Male Sprague-Dawley rats (Japan SLC, Kyoto, Japan, 10 wk old, *n* = 11) were anesthetized with pentobarbital sodium (Nembutal, Dainippon Sumitomo Pharma, Osaka, Japan, 50 mg/kg ip) and artificially ventilated (4 ml tidal volume, 57 breaths/min). Body temperature was maintained at 36–38°C with the use of a heating pad. A maintenance infusion of lactated Ringer solution (Otsuka Pharmaceuticals, Osaka, Japan) containing 3 mg/ml pentobarbital sodium was delivered intravenously via a jugular vein at 4 ml/h. Intraperitoneal boluses of pentobarbital were also administered as required to maintain deep anesthesia.

Arterial pressure was recorded via a catheter placed in a carotid artery. A catheter (polyvinyl chloride, outer diameter 0.5 mm, inner diameter 0.2 mm, with a heat-stretched tip) was inserted into the left femoral artery and advanced up the aorta so that its tip lay just above the level of the left renal artery. The left kidney was approached via a retroperitoneal incision. It was freed from the peritoneal lining and surrounding fat and placed in an acrylic restraining cup held by a micromanipulator. The femoral artery catheter was then manipulated so that its tip lay in the left renal artery. This catheter was later used for contrast agent administration. In some animals that received

Address for reprint requests and other correspondence: G. Eppel, Dept. of Physiology, PO Box 13F, Monash Univ., VIC 3800, Australia (e-mail: gabriela.eppel@med.monash.edu.au).

angiotensin II or vehicle treatment, a transit time flow probe (1RB, Transonic Systems, Ithaca, NY) was placed around the left renal artery for measurement of renal blood flow (RBF). For animals in which the renal nerves were electrically stimulated, the major renal nerve trunks alongside the left renal artery were identified by use of a surgical microscope and placed across a pair of hooked stimulating electrodes. The nerves were then sectioned upstream of the electrode. Petroleum jelly was applied to the nerves throughout the experiment to prevent dehydration. Electrical stimulation of the renal nerves (RNS) was produced by use of purpose-written software in the LabVIEW graphical programming language (Universal Stimulator, University of Auckland, New Zealand) coupled to a LabPC+ data-acquisition board (National Instruments, Austin, TX).

Once surgical preparation was complete, the rat was moved into the X-ray hutch. The rat was placed on its side and the kidney was exteriorized by adjusting the position of the kidney cup so that the kidney was in line with the horizontal X-ray beam and the detector system. An intramuscular injection of the neuromuscular blocker pancuronium bromide (Mioblock, Sankyo, Tokyo, Japan, 2 mg/kg) was administered after confirmation of deep anesthesia. The neuromuscular blocker was necessary to prevent movement artifacts from breathing movements during interruptions in ventilation for angiogram recordings.

Contrast administration. Iodinated contrast medium (Iomeron 350; Eisai, Tokyo, Japan) containing ~0.5 IU of heparin per bolus was injected into the left renal artery with a clinical autoinjector (Nemoto Kyorindo, Tokyo, Japan). To overcome the resistance of the catheter to rapid delivery of the viscous contrast agent, a nominal minimum bolus greater than 0.1 ml was required. We observed that 20–30 μl of the contrast was delivered as a bolus at a rate no less than 10 μl/s. The contrast agent continued to exit the catheter at a slower rate for some time after the initial bolus due to back pressure. The transit time of the initial bolus through the arterial circulation was ~1 s. At the same time as the bolus was injected, image recording commenced and the ventilator was turned off for a few seconds to reduce movement artifacts in the images. We observed that contrast agent delivered into the renal artery was dispersed into discrete regions of the kidney

rather than the entire kidney, likely reflecting plasma streaming (23). Therefore, one to three boluses were initially administered to identify the best region of the kidney to image. The first angiogram obtained in the chosen region was used as the control angiogram. Once an angiogram was collected, a 20- to 30-min recovery period was allowed before the next bolus was administered.

Experimental protocol. Three groups of rats were studied. In each group a control angiogram was first obtained. Then the rats received one of three treatments *1*) intravenous infusion of angiotensin II (1,600 ng·kg^{-1}·min^{-1}, *n* = 4), *2*) vehicle administration (0.9% NaCl, 2.4 ml/h iv, *n* = 4) or *3*) electrical stimulation of the renal nerves (RNS, *n* = 3). Angiotensin II and vehicle administration continued for 10–15 min before contrast bolus administration was repeated. RNS was performed at 10 V (supramaximal voltage), 2 Hz with a pulse width of 2 ms for a period of 3 min. Contrast agent was administered 45 s after RNS began. RBF responses to RNS have previously been observed to stabilize by this time point (G. A. Eppel, unpublished observation).

Data acquisition and processing. The carotid artery catheter was connected to a pressure transducer (Cobe, Arvarda, CO). The transit-time ultrasound flow probe was connected to a compatible flowmeter (T106, Transonic Systems). These analog signals were digitized at 500 Hz and continuously displayed by a data-acquisition program (Universal Acquisition, University of Auckland, New Zealand), allowing continuous sampling and recording of mean arterial pressure (MAP, mmHg), heart rate (HR, beats/min, derived from the MAP waveform), and RBF (ml/min).

The X-ray detector system has been described previously (30). Briefly, synchrotron radiation has a broad and continuous spectrum. A crystal monochromator selects a single energy of radiation. A rotating-disk X-ray shutter, which is situated between the monochromator and the object of interest, produces pulsed monochromatic X-rays. After transmission through the object, X-rays are detected by using the SATICON image detector. Images (1,024 × 1,024 pixels) were recorded at a rate of 30 frames per second for 3.3–8.3 s and stored in 10-bit format. The input field (field of view) of the X-ray SATICON camera (Hamamatsu Photonics, Hamamatsu, Japan) was 7.0 × 7.0

Fig. 1. Image processing for the determination of blood vessel diameter. From a single original frame a region of interest was selected (blue rectangle, *A*). A tungsten wire with a diameter of 100 μm (14 pixels) was present in the top corner of each image and was used for software calibration. A background image was subtracted from the region of interest (*B*, grayscale inverted) and the resultant image was contrast enhanced using purpose-written software (*C*, grayscale; *D*, color). A line 5 pixels wide (35 μm) was drawn across a vessel of interest (*E*, subregion of *D*). The intensity profile of the line was then used for further analysis (Fig. 5). The yellow lines in *B* indicate the designation of 1 vessel for the purposes of the measurement of diameter.
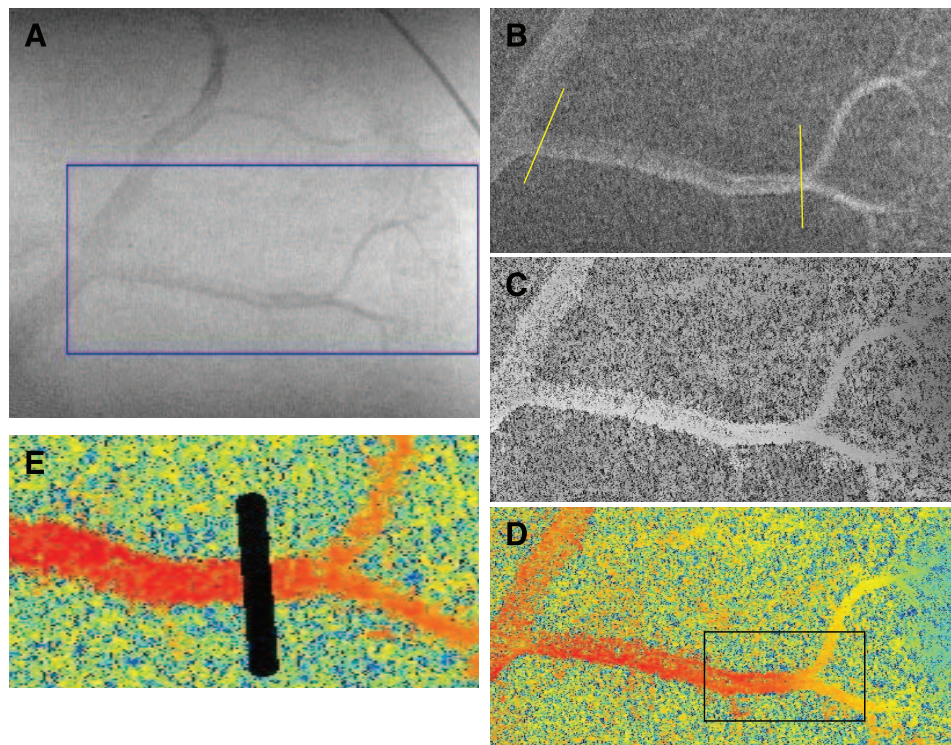
mm (1 pixel = ~7 μm). Shutter open time was 2.6–3.0 ms. Monochromatic X-ray energy was adjusted to 33.2 keV, just above the iodine K-edge energy for maximal contrast.

For enhanced clarity, some figures in the manuscript were prepared by subtracting an averaged precontrast background frame from the average of sequential frames. Finally, a Gaussian filter (3 × 3 pixels) was applied (Image J software, National Institutes of Health).

Measurements of vessel lumen diameter. To process images for the determination of blood vessel diameter, a region of interest was selected from a single original frame (Fig. 1). A background image, defined as the average of five frames collected prior to the vasculature filling with contrast agent, was automatically subtracted from subsequent images taken during and after contrast administration. The background-corrected images were automatically contrast enhanced by morphological filtering-based algorithms. A full example of this approach can be found in the work of Zana and Klein (34, 35). In short, the algorithm is based on the assumptions that *1*) images of the vessels have a Gaussian shape in cross section, *2*) vessels are linear within the region of interest, and *3*) vessels are spaced apart from each other. From this, a set of linear structuring elements are used with "opening" and "top-hat" operations (34, 35). It becomes possible to brighten the vessels that correspond to the orientation of the structuring element by summing a series of top-hat operations. The process was greatly simplified by focusing on particular vessels. The structuring element was typically 200 pixels long and orientated over a range of angles (10° intervals).

Once a region of interest was contrast enhanced, a line 5 pixels (35 μm) wide was drawn across a vessel of interest to obtain an intensity profile averaged across the 5 pixels (Fig. 1). A temporal average of the intensity profile of this line over 40 frames was also produced (Fig. 2). A sequence of frames was chosen in which the vessel of interest was most intensely filled with contrast agent. The edges of the vessels were defined by the steepest change in intensity along the averaged line profile. These data were processed with an in-house code by use of MatLab (The MathWorks, MA), which automated the processes of background subtraction, contrast enhancement, line profile production and averaging, and simplified setting of lines to profile and the selection of frames to analyze.

The number of measurements obtained for each vessel was dependent on vessel length (1 measurement per mm of vessel length). A vessel was defined as one continuous length, even when smaller vessels branched from it, provided the branching did not result in a major change in the size of the continuing vessel. For example, in Fig. 1*B*, the length of one vessel was designated to be from its origin at a larger vessel to a bifurcation where the two branches were about half the size of the parent vessel. The line profiles for the measurements were obtained at approximately equally spaced points (i.e., every 1 mm) along the length of vessels. In cases where only one measurement was made per vessel, the line profile was set at, or as close as possible to, the midpoint of the vessel length. Tungsten wire with a diameter of 100 μm, present in the top corner of each original image, was used for software calibration.

Measurements of glomerular diameter. Measurements were performed on single original frames from the control period. A line profile was set across each glomerulus. In-house code (MatLab) was programmed to generate the line profile of the corresponding perpendicular line across the center of the glomerulus. The lengths over which these lines were superimposed over the glomerulus were averaged for each glomerulus. Diameters were determined for five glomeruli in each of five kidneys. The diameters were averaged per kidney and subsequently across the five kidneys.

Statistical analyses. All hemodynamic variables and measurements of glomerular diameter are expressed as between-animal means ± SE. When multiple measurements of lumen diameter were made along the length of specific vessels, these were averaged to provide mean lumen diameter for the vessel. For analytic purposes, vessels were binned according to basal lumen diameter (<101, 101–200, or >200 μm)
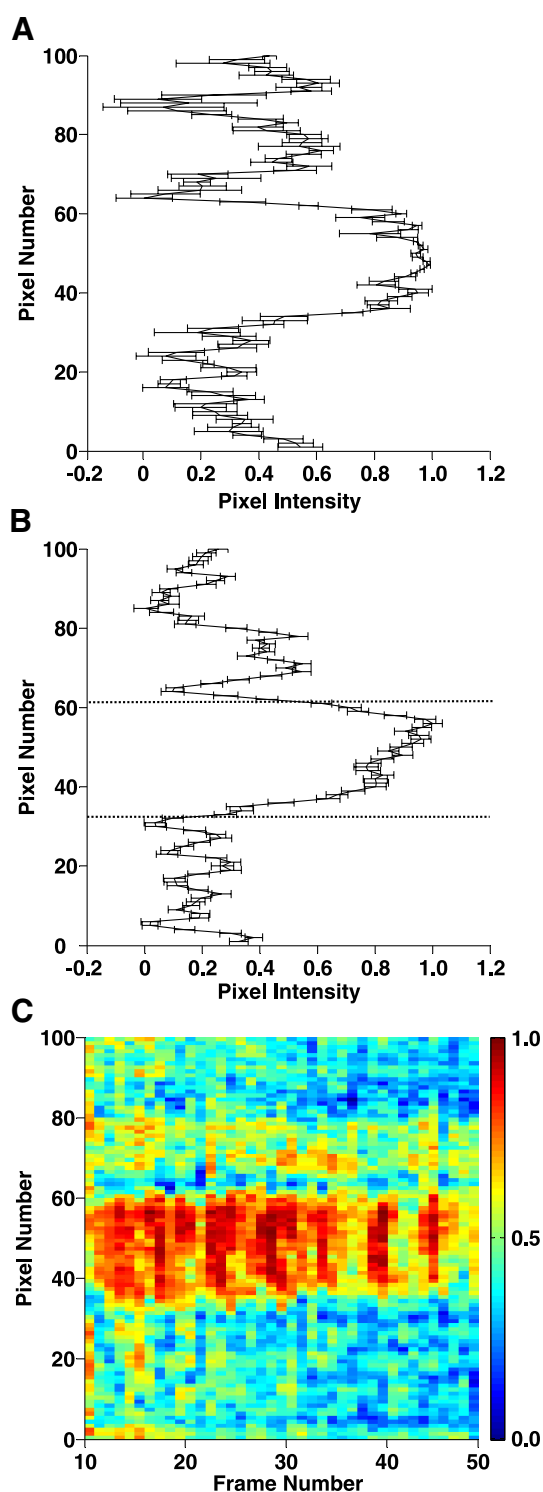

Fig. 2. Determination of blood vessel diameter. The intensity profile from a single frame of a line (5 pixels wide) across a vessel (*A*, means ± SE, *n* = 5 pixels). An averaged profile of the same line over a series of 40 frames (*B*, means ± SE, *n* = 40 frames). The dotted lines indicate the vessel edges. *C* presents the line profile over the same series of 40 frames as in *B*, with color reflecting pixel intensity.

and data are presented as between-vessel means ± SE. Parallel analyses of these data were also performed with individual animals, rather than individual vessels, being the experimental unit. Results were similar by both approaches. Hypothesis testing was performed

by Student's paired *t*-test. Two-sided $P \leq 0.05$ was considered statistically significant.

RESULTS

Effects of contrast bolus administration on baseline hemodynamic variables. Prior to collection of the control angiograms the average MAP in all rats was 103 ± 5 mmHg and HR was 393 ± 12 beats/min ($n = 11$). Injection of contrast agent into the renal artery resulted in a transient increase in MAP (Fig. 3). Within the first 2–6 s after bolus delivery, the increase in MAP peaked at 7 ± 1 mmHg above baseline. HR was not significantly altered (-2 ± 1 beats/min). It was in this time frame that most images used for analysis of arterial lumen diameters were collected. MAP subsequently decreased to below baseline at some stage during the period 10–24 s after contrast injection. It then rose again more gradually, reaching a plateau 17 ± 4 mmHg above baseline within 5 min of bolus administration. At this point HR was reduced by 8 ± 3 beats/min. A 20- to 30-min recovery period was required for MAP to return to levels close to baseline.

Table 1. *Basal hemodynamic variables*

Group and Period	Mean Arterial Pressure, mmHg	Heart Rate, beats/min
Vehicle ($n = 4$)		
Control	93 ± 9	384 ± 26
Vehicle	85 ± 6	367 ± 27
AngII ($n = 4$)		
Control	117 ± 7	423 ± 15
AngII	114 ± 13	423 ± 28
RNS ($n = 3$)		
Control	105 ± 7	384 ± 10
RNS	111 ± 11	390 ± 22

Values are means $\pm$ SE of recordings during the 30 s prior to contrast administration. AngII, angiotensin II; RNS, electrical stimulation of the renal nerves.

Effects of vehicle treatment, angiotensin II, and renal nerve stimulation on baseline hemodynamic variables. Administration of the saline vehicle did not significantly affect baseline MAP or HR (Table 1). RBF was 2.0 ± 0.7 ml/min during the control period and 2.2 ± 0.7 ml/min during vehicle administration ($n = 4$). Administration of angiotensin II initially raised
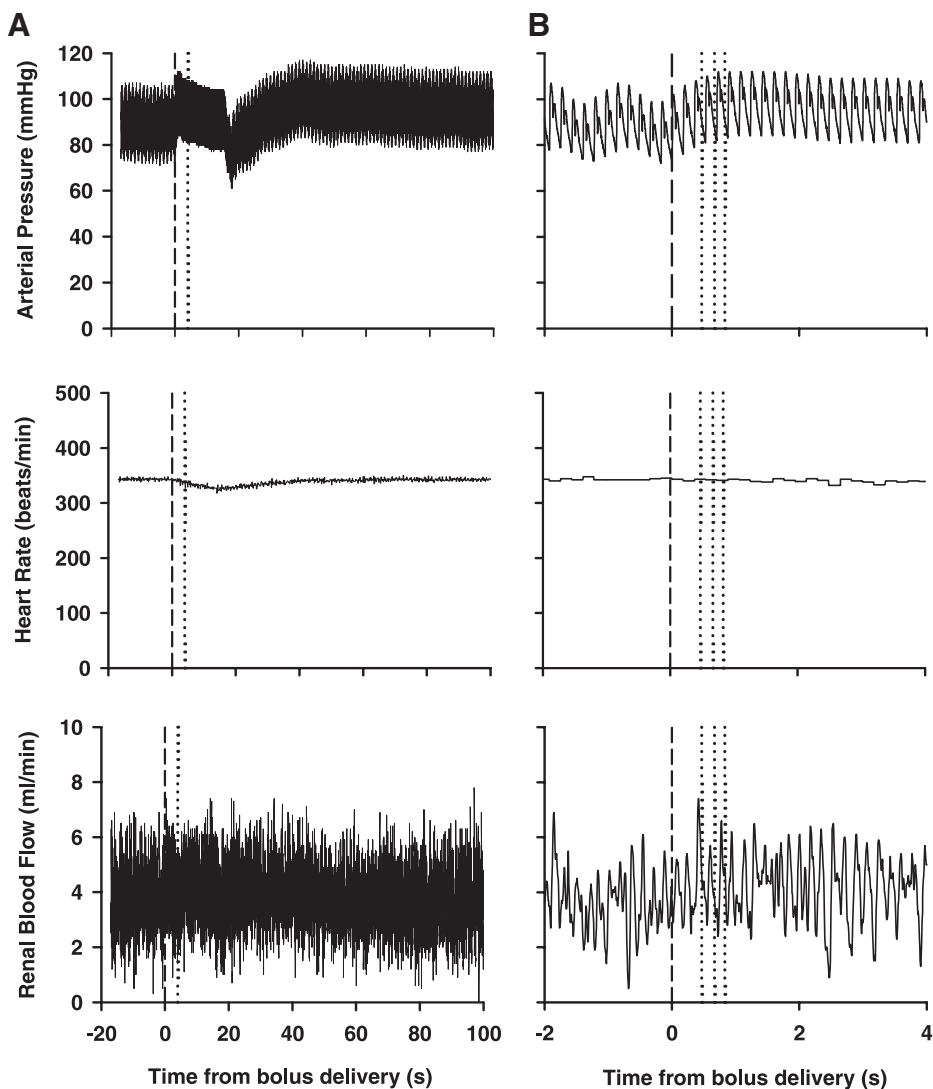

Fig. 3. Typical hemodynamic responses to bolus administration of contrast agent. *A* demonstrates the responses over a period of 100 s. The dotted line indicates 4 s from bolus administration, which is the time frame shown in *B*. The dotted lines in *B* refer to the time points at which the frames in Fig. 5 were collected (0.47, 0.67, and 0.83 s).

MAP by 29 ± 6 mmHg during the first 10–20 min of the infusion. However, this pressor effect waned so that MAP during the period immediately before the effects of angiotensin II on vessel caliber were determined was not significantly different from that during the control period. RBF was measured in two of the animals treated with angiotensin II. Angiotensin II reduced RBF by 65% in one rat (from 3.4 to 1.2 ml/min) and by 61% in the other (from 2.8 to 1.0 ml/min). RBF remained at this level throughout the equilibration period and during injection of contrast medium.

RNS did not alter MAP or HR relative to their initial baseline values. It was not possible to perform RNS and simultaneously measure RBF in the present study, since there was insufficient space along the length of the left renal artery for the intrarenal arterial catheter and stimulating electrode plus a perivascular flow probe. However, in preliminary experiments (with no intrarenal arterial catheter) in which RBF responses to RNS were measured, RNS at 10 V and 2 Hz reduced RBF by 20–35% ($n = 2$). We expect that similar reductions occurred in response to RNS in the animals from which we collected angiograms. In all cases of the present study RNS at 10 V and 8 Hz blanched the kidney, indicating that the nerves were functional.

Contrast angiograms. Within the first 1 s after bolus delivery, regions of the preglomerular vasculature were clearly visible (Fig. 4*A*). Up to four levels of branching could be observed along the arterial tree. The contrast agent initially filled the arterial circulation and was then gradually transferred to the glomeruli, tubules, and postglomerular vasculature, obscuring the preglomerular vascular tree (Fig. 4, *B* and *C*). Individual glomeruli were clearly visible in some angiograms. Arterial lumen diameters were measured over a sequence of 40 frames, typically the 10th to 49th frames (0.3 to 1.67 s) from contrast injection. In this time range, the arterial circulation was filled with contrast agent and was clearly visible. The diameters measured over these 40 frames were averaged. Lumen diameter measurements ranged from 28 to 400 μm.

Effects of vehicle treatment, angiotensin II, and renal nerve stimulation on vascular lumen diameters. Typical angiograms taken before and during treatment with vehicle, angiotensin II, and RNS are shown in Fig. 5. Visual inspection of these images indicates that vascular caliber was little affected by vehicle treatment, but as expected was reduced during angiotensin II infusion and RNS. This was confirmed by our quantitative analysis (Fig. 6). Average lumen diameter (across all vessels) did not change significantly from the control period to the vehicle treatment period (+3.1 ± 3.5% for all data, $P = 0.4$, Fig. 6). During angiotensin II treatment there were significant reductions in vascular lumen diameters. On average, vessel diameter decreased by 24.3 ± 3.4% ($P < 0.001$). The response to angiotensin II was similar across all vessels independent of size (Figs. 5, *C* and *D*, and 6*B*). During renal nerve stimulation vascular lumen diameters were also significantly reduced, on average by 17.1 ± 3.8% ($P < 0.001$). However, when these data were binned according to vessel size this effect was only significant for vessels 101–200 μm in diameter (Figs. 5, *E* and *F*, and 6*C*). The reductions were less pronounced for other vessel sizes, particularly for vessels 40–100 μm in diameter.

Glomerular diameters. Glomerular diameters were measured over a sequence of frames, typically from the 80th to 120th frames obtained 2.6–4 s after contrast injection. The
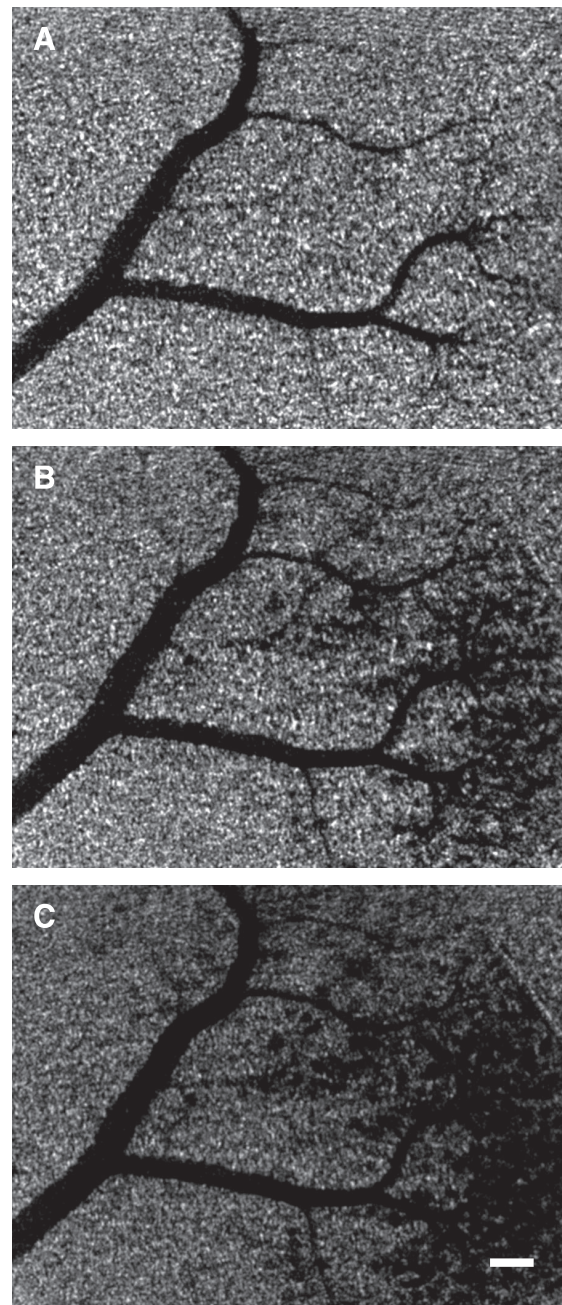

Fig. 4. Contrast angiograms of the renal circulation collected 0.33–0.46 s (*A*), 0.50–0.66 s (*B*), and 0.69–0.83 s (*C*) from contrast delivery. These images are averages of frames that have been background subtracted. The averaged frames were subsequently filtered by use of a Gaussian filter (3×3 pixels) using Image J (National Institutes of Health). Calibration bar represents 500 μm.

diameters averaged 202 ± 24 μm ($n = 5$ kidneys). Glomerular dimensions were not determined during vehicle, angiotensin II, or RNS treatments.

DISCUSSION

To our knowledge this is the first description of a method that allows simultaneous measurement of the lumen diameters of renal feeding arteries and interlobar, arcuate, and interlobular arteries and allows repeated measurements to be made of specific vessels within the same animal. Our method also
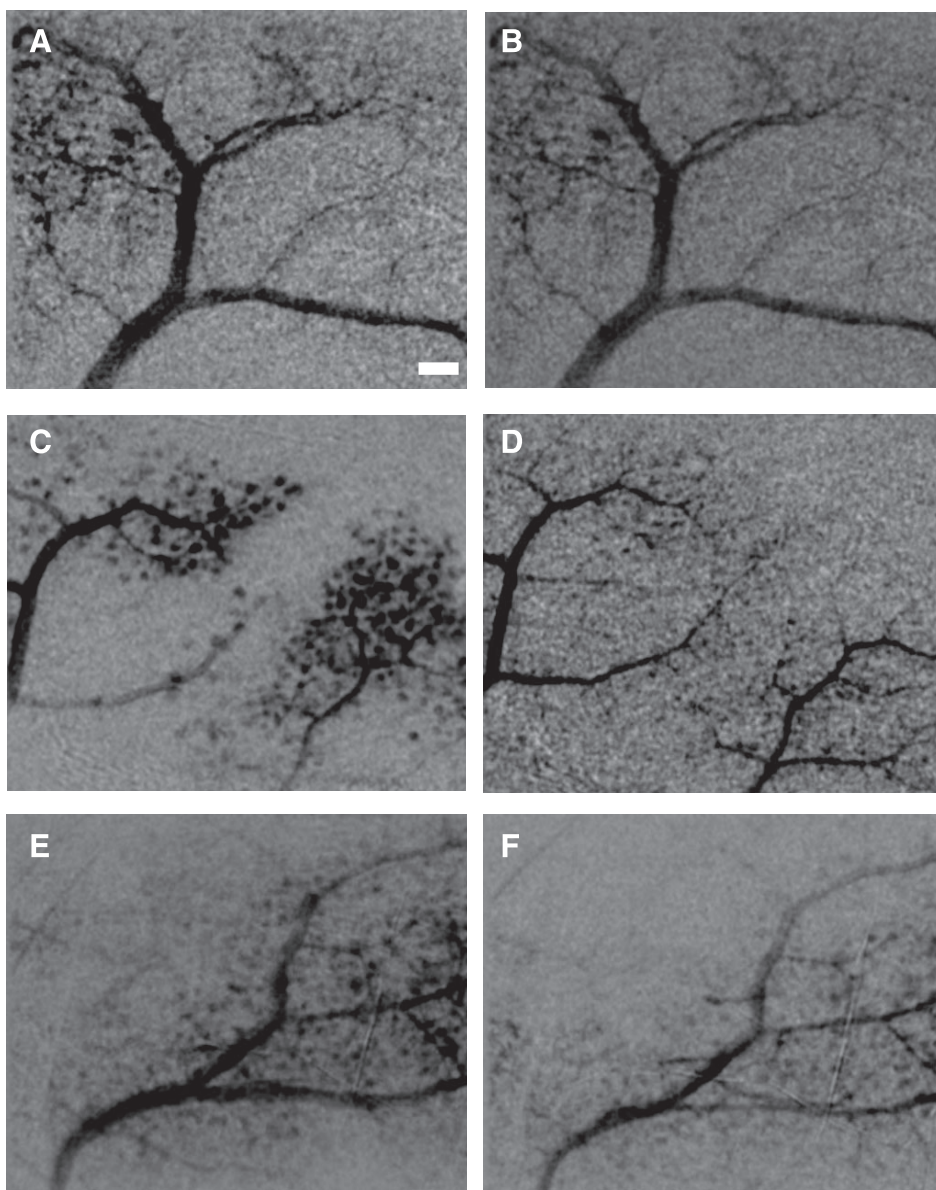
Fig. 5. Effects of vehicle treatment, angiotensin II, and renal nerve stimulation on renal angiograms. *A*, *C*, and *E* were collected under control conditions; *B*, *D*, and *F* were collected during vehicle treatment, angiotensin II infusion, and renal nerve stimulation, respectively. The images have been processed as for Fig. 2. The images presented in corresponding *left* and *right* panels were collected at equivalent time points following contrast injection. Calibration bar represents 500 μm.

allows repeated measurement of glomerular diameter (capillaries plus Bowman's capsule). Recordings of the renal vasculature were made after small boluses of concentrated iodine containing contrast agent were injected directly into the renal artery. Measurements of the preglomerular vascular tree were made prior to the agent passing into the glomeruli. Measurements of glomerular diameter were made at a later time point when the glomeruli were full of contrast agent. By using this procedure, repeated boluses were tolerated without deterioration of the preparation, provided there was a 20- to 30-min recovery period after each bolus. Background subtraction eliminated the majority of signal noise to achieve a flat-field correction. Purpose-written software enabled contrast enhancement and automation of edge detection over multiple frames, at multiple points along vessels and over vessel regions several pixels wide, reducing measurement error and variability.

Our measurements of vascular diameter are in close agreement with those obtained from the ex vivo juxtamedullary nephron preparation (11), perfusion-fixed histological sections,

(29) and microcomputer tomography of vascular casts (22). Our measurements of mean glomerular diameter are similar to those from perfusion-fixed histological sections of the rat kidney, which have been found to vary from ~150–190 μm depending on the depth of the glomeruli within the cortex (24). We did not measure glomerular responses to the vehicle, angiotensin II, or RNS because the effects of these treatments on glomerular dimensions are likely to be small (15) and not within the detectable range of this technique. Nevertheless, we see considerable scope for the use of this technique for assessment of structurally based changes in glomerular dimensions that develop over longer time periods. For example, it should be possible to monitor development of glomerular hypertrophy such as occurs in animal models of hypertension or nephron deficiency (28). However, this would first require the development of a less invasive method for contrast delivery.

The classical anatomical classification of renal arterial elements into interlobar, arcuate, and interlobular arteries is based on a somewhat idealized concept of renal vascular anatomy
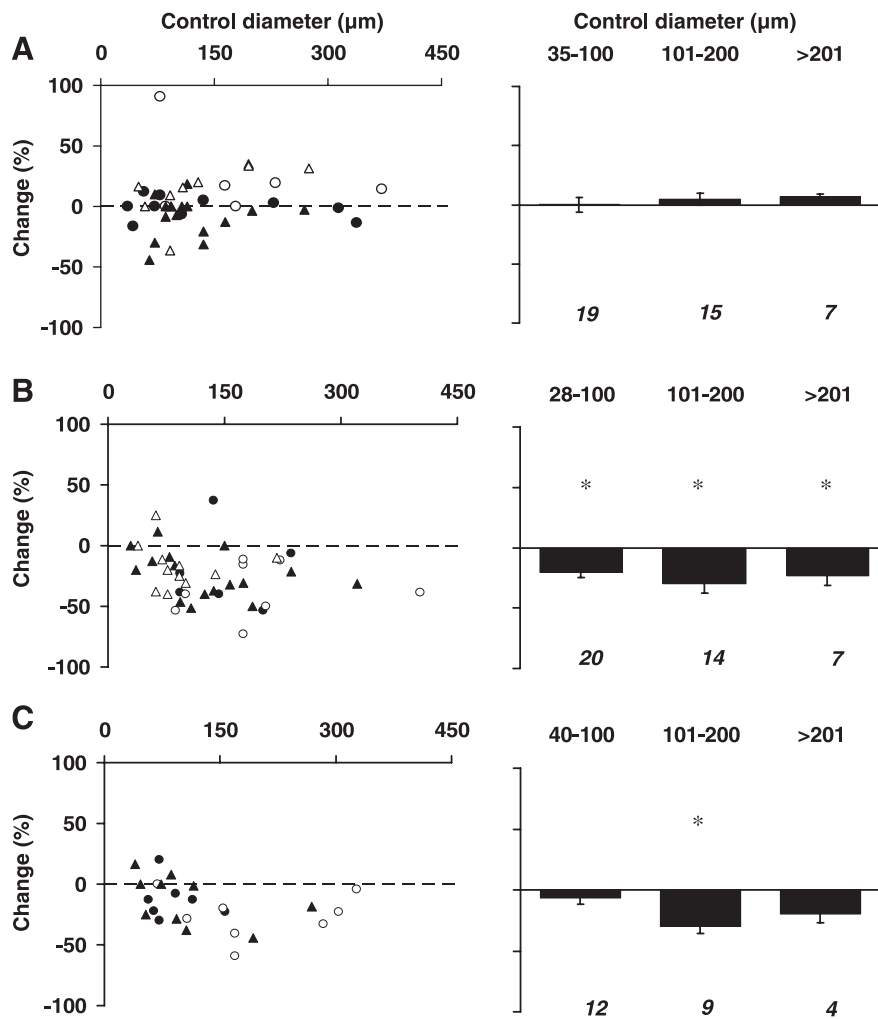
Fig. 6. Changes in vessel diameter in response to vehicle treatment (*A*), angiotensin II treatment (*B*), and renal nerve stimulation (*C*). *Left*: raw data. Each point represents a single vessel. Within each graph, data points represented by the same symbol were collected from the same rat. *Right*: data binned according to vessel size (means ± SE). Numbers in italics indicate the number of vessels included in each bin. Data from all rats have been combined on the *right*. *$P \leq 0.001$ as determined from the *t*-distribution.

(10), so in reality it has only limited analytical utility. A recent structural analysis of the rat renal vasculature by Nordsletten and colleagues (22) has further refined our understanding of renal vascular architecture, through the classification of renal vessels according to Strahler order. Afferent arterioles were defined as arterial vessels of Strahler order 0 and 1, having mean lumen diameters ranging from ∼10 to ∼14 μm, respectively. Vessels of Strahler order 2–6 (∼20 to ∼55 μm) were considered to be mostly interlobular arteries, arcuate arteries were considered to include vessels of Strahler order 6–7 (∼55–85 μm), interlobar vessels were considered to include vessels of Strahler order 8 and 9 (∼140 to 190 μm), and feeding renal arteries were considered to include Strahler orders 9 and 10 (∼190 to 215 μm). In our present analysis, we placed vessels in bins according to their lumen diameter under baseline conditions. Application of Nordsletten et al.'s approach to our present analysis suggests that the vessels placed in the <101-μm bin likely comprise mostly interlobular and arcuate arteries, vessels in the 100-200-μm bin likely comprise mostly interlobar arteries, and vessels of diameter greater than 200 μm likely comprise mostly feeding renal arteries. The visualization and measurement of afferent and efferent arterioles is currently beyond the limits of the technique. Therefore we cannot draw conclusions about the responses of these vessels to the various treatments. In the future, the develop-

ment of highly opaque contrast agents with low viscosity may improve contrast concentration in smaller vessels, but an improved spatial resolution of the detector system would also be required to extend the limits of the technique. Such refinements would allow measurement of afferent and efferent arteriole caliber. Subsequently this would allow computation of the contributions of various vascular elements to total renal vascular conductance and thereby a truly quantitative analysis of control of global and regional renal perfusion under in vivo conditions.

Previous investigations of the heterogeneity of renal vascular responses to vasoactive agents have mainly focused on the differential responsiveness of afferent and efferent arterioles, which appears critical for fine regulation of glomerular filtration (21). For example, some factors appear to act predominantly at the level of the efferent arteriole, like the vasodilator anandamide (16), whereas others appear to act predominantly at the afferent arteriole, such as endothelium-derived hyperpolarizing factor (32). There is also evidence of differential sensitivity to vasoactive agents of glomerular arterioles in the juxtamedullary cortex compared with those in more superficial regions of the cortex (17), which may in turn contribute to the physiological regulation of the distribution of blood flow between the renal cortex and medulla (8). However, to date there has been relatively little investigation for the potential for

heterogeneity of the responsiveness of arterial vascular elements in the kidney, which could also potentially contribute to the physiological regulation of regional kidney perfusion and glomerular filtration (8). Those studies that have been reported have mainly employed the hydronephrotic kidney model, which allows direct visualization of nearly the entire renal microvasculature, albeit in a chronically nonfiltering and remodeled kidney. For example, van Rodijnen and colleagues (31) recently showed that proximal interlobular arteries constrict in response to prostaglandin E2, whereas downstream vascular elements tend to dilate.

In our present study, we found that the magnitude of vasoconstriction in response to angiotensin II was relatively constant across the preglomerular arterial circulation. These findings extend those of Carmines and colleagues (2), who observed similar responses to angiotensin II of arcuate and interlobular arteries (which they did not distinguish) and both afferent and efferent arterioles using the blood perfused juxtamedullary nephron preparation. Furthermore, in the split hydronephrotic kidney, Dietrich et al. (7) observed similar vasoconstrictor responses to angiotensin II in arcuate arteries, interlobular arteries, afferent arterioles and efferent arterioles. In the rabbit kidney in vivo, Denton et al. (4) observed similar responses to angiotensin II of interlobular arteries and afferent and efferent arterioles, based on a cross-sectional analysis of vascular casts taken from rabbits in which either angiotensin II or saline was administered into the renal artery. Taken collectively, these data provide strong evidence that the sensitivity to angiotensin II is relatively homogeneous across the length of the renal arterial and arteriolar vasculature. The significance of our present finding is that it was made by longitudinal observations of specific vessels in vivo in morphologically and physiologically normal kidneys. Furthermore, our present observations extend from interlobular vessels all the way upstream to the feeding arteries that branch from the main renal artery.

In contrast to our findings with angiotensin II, vasoconstriction in response to RNS appeared to be heterogeneous across the renal arterial circulation. RNS significantly reduced vessel diameter in vessels having a resting caliber of 101–200 μm ($-30 \pm 6\%$). This response was of a similar magnitude to the response to angiotensin II in vessels of the same size ($-30 \pm 7\%$). In contrast, RNS had little effect on vascular tone in vessels with a resting caliber of 40–100 μm ($-7 \pm 5\%$). Responses to RNS of vessels of resting caliber greater than 201 μm may also have been relatively weak ($-20 \pm 12\%$), although we must apply considerable caution to the interpretation of these data because of the limited number of observations we were able to make of these larger vessels. Nevertheless, our data support the notion that interlobular and perhaps also arcuate arteries might be less sensitive than interlobar arteries to the effects of RNS. It should be noted that our data are not at odds with the strong evidence that afferent arterioles are highly sensitive to the effects of renal nerve stimulation (3, 6).

There were some differences in resting MAP between the three groups of rats we studied. In particular, resting MAP was somewhat lower in the vehicle group than in the other groups. However, resting MAP was not significantly different in the rats treated with angiotensin II compared with those in which the renal nerves were stimulated. Thus variations in basal MAP

are unlikely to have had a major impact on our observations of the effects of these treatments on vascular caliber.

Microangiography using synchrotron radiation has recently been applied to a range of vascular beds (27), including the liver (14), lungs (25, 26), brain (13, 18–20, 30), and heart (12). One of the major the strengths of the technique is that there is no geometric magnification of vessels. The highly collimated X-ray beam, the small X-ray source, and the long distance between the source and the kidney result in insignificant magnification of blood vessels due to their relative position within the organ of interest (i.e., ×1.004) (26). As for other vascular imaging modalities (34), analysis of microangiograms assumes all arterial vessel segments are cylindrical in shape. As such, the measured radius of the vessels should be the same regardless of the orientation of the vessels in three dimensions provided the vessels are not parallel to the X-ray beam. Vessels parallel to the beam are not generally included in analyses. Therefore microangiography provides measurements of vascular diameter that are little affected by the relative distance or orientation of individual vessels or vessel segments to the camera or X-ray source. To our knowledge there have been no previous synchrotron-based investigations of the behavior of the renal microvasculature in vivo. Our present findings show that such studies are feasible. Indeed, our method has allowed us to follow changes in vascular lumen dimensions, along the branching structure of the renal vasculature, in response to both angiotensin II and RNS. Our long-term goal is to use this method along with the recent structural analysis of the renal vasculature (22) to provide a complete analysis of the contributions of different vascular elements to segmental vascular tone. This will require increased resolution so we can visualize and measure caliber of all vascular elements down to the level of the afferent and efferent arterioles.

REFERENCES

1. **Bentley MD, Ortiz MC, Ritman EL, Romero JC.** The use of micro-computed tomography to study microvasculature in small rodents. *Am J Physiol Regul Integr Comp Physiol* 282: R1267–R1279, 2002.
2. **Carmines PK, Morrison TK, Navar LG.** Angiotensin II effects on microvascular diameters of in vitro blood-perfused juxtamedullary nephrons. *Am J Physiol Renal Fluid Electrolyte Physiol* 251: F610–F618, 1986.
3. **Chen J, Fleming JT.** Juxtamedullary afferent and efferent arterioles constrict to renal nerve stimulation. *Kidney Int* 44: 684–691, 1993.

4. **Denton KM, Anderson WP, Sinniah R.** Effects of angiotensin II on regional afferent and efferent arteriole dimensions and the glomerular pole. *Am J Physiol Regul Integr Comp Physiol* 279: R629–R638, 2000.

5. **Denton KM, Shweta A, Finkelstein L, Flower RL, Evans RG.** Effect of endothelin-1 on regional kidney blood flow and renal arteriole calibre in rabbits. *Clin Exp Pharmacol Physiol* 31: 494–501, 2004.

6. **DiBona GF, Kopp UC.** Neural control of renal function. *Physiol Rev* 77: 75–197, 1997.

7. **Dietrich MS, Endlich K, Parekh N, Steinhausen M.** Interaction between adenosine and angiotensin II in renal microcirculation. *Microvasc Res* 41: 275–288, 1991.

8. **Evans RG, Eppel GA, Anderson WP, Denton KM.** Mechanisms underlying the differential control of blood flow in the renal medulla and cortex. *J Hypertens* 22: 1439–1451, 2004.

9. **Evans RG, Majid DS, Eppel GA.** Mechanisms mediating pressure natriuresis: what we know and what we need to find out. *Clin Exp Pharmacol Physiol* 32: 400–409, 2005.

10. **Fourman J, Moffatt DB.** *The Blood Vessels of the Kidney*. Oxford, UK: Blackwell Scientific, 1971.

11. **Inscho EW.** P2 receptors in regulation of renal microvascular function. *Am J Physiol Renal Physiol* 280: F927–F944, 2001.

12. **Iwasaki H, Fukushima K, Kawamoto A, Umetani K, Oyamada A, Hayashi S, Matsumoto T, Ishikawa M, Shibata T, Nishimura H, Hirai H, Mifune Y, Horii M, Sugimura K, Suehiro S, Asahara T.** Synchrotron radiation coronary microangiography for morphometric and physiological evaluation of myocardial neovascularization induced by endothelial progenitor cell transplantation. *Arterioscler Thromb Vasc Biol* 27: 1326–1333, 2007.

13. **Kidoguchi K, Tamaki M, Mizobe T, Koyama J, Kondoh T, Kohmura E, Sakurai T, Yokono K, Umetani K.** In vivo x-ray angiography in the mouse brain using synchrotron radiation. *Stroke* 37: 1856–1861, 2006.

14. **Kobayashi S, Hori M, Dono K, Nagano H, Umeshita K, Nakamori S, Sakon M, Osuga K, Umetani K, Murakami T, Nakamura H, Monden M.** In vivo real-time microangiography of the liver in mice using synchrotron radiation. *J Hepatol* 40: 405–408, 2004.

15. **Kon V, Karnovsky MJ.** Morphologic demonstration of adrenergic influences on the glomerulus. *Am J Pathol* 134: 1039–1046, 1989.

16. **Koura Y, Ichihara A, Tada Y, Kaneshiro Y, Okada H, Temm CJ, Hayashi M, Saruta T.** Anandamide decreases glomerular filtration rate through predominant vasodilation of efferent arterioles in rat kidneys. *J Am Soc Nephrol* 15: 1488–1494, 2004.

17. **Matsuda H, Hayashi K, Wakino S, Kubota E, Honda M, Tokuyama H, Takamatsu I, Tatematsu S, Saruta T.** Role of endothelium-derived hyperpolarizing factor in ACE inhibitor-induced renal vasodilation in vivo. *Hypertension* 43: 603–609, 2004.

18. **Morishita A, Kondoh T, Sakurai T, Ikeda M, Bhattacharjee AK, Nakajima K, Kohmura E, Yokono K, Umetani K.** Quantification of distension in rat cerebral perforating arteries. *Neuroreport* 17: 1549–1553, 2006.

19. **Morita M, Ohkawa M, Miyazaki S, Ishimaru T, Umetani K, Suzuki K.** Simultaneous observation of superficial cortical and intracerebral microvessels in vivo during reperfusion after transient forebrain ischemia in rats using synchrotron radiation. *Brain Res* 1158: 116–122, 2007.

20. **Myojin K, Taguchi A, Umetani K, Fukushima K, Nishiura N, Matsuyama T, Kimura H, Stern DM, Imai Y, Mori H.** Visualization of intracerebral arteries by synchrotron radiation microangiography. *Am J Neuroradiol* 28: 953–957, 2007.

21. **Navar LG, Inscho EW, Majid SA, Imig JD, Harrison-Bernard LM, Mitchell KD.** Paracrine regulation of the renal microcirculation. *Physiol Rev* 76: 425–536, 1996.

22. **Nordsletten DA, Blackett S, Bentley MD, Ritman EL, Smith NP.** Structural morphology of renal vasculature. *Am J Physiol Heart Circ Physiol* 291: H296–H309, 2006.

23. **Parekh N.** A novel method for infusing drugs continuously into the renal artery of rats. *Am J Physiol Renal Fluid Electrolyte Physiol* 268: F967–F971, 1995.

24. **Sands JM, Kokko JP, Jacobson HR.** Inrarenal heterogeneity: vascular and tubular. In: *The Kidney: Physiology and Pathophysiology*, edited by Seldin DW and Giebsich G. New York: Raven, 1992, p. 1087–1155.

25. **Schwenke DO, Pearson JT, Kangawa K, Umetani K, Shirai M.** Changes in macrovessel pulmonary blood flow distribution following chronic hypoxia: assessed using synchrotron radiation microangiography. *J Appl Physiol* 104: 88–96, 2008.

26. **Schwenke DO, Pearson JT, Umetani K, Kangawa K, Shirai M.** Imaging of the pulmonary circulation in the closed-chest rat using synchrotron radiation microangiography. *J Appl Physiol* 102: 787–793, 2007.

27. **Shirai MSD, Eppel GA, Evans RG, Edgley AJ, Tsuchimochi H, Umetani K, Pearson JT.** Synchrotron based angiography for investigating regulation of vasomotor function in the microcirculation in vivo. *Clin Exp Pharmacol Physiol* 36: 107–116, 2009.

28. **Shweta A, Cullen-McEwen LA, Kett MM, Evans RG, Denton KM, Fitzgerald SM, Anderson WP, Bertram JF.** Glomerular surface area is normalized in mice born with a nephron deficit: no role for AT_1 receptors. *Am J Physiol Renal Physiol* 296: F583–F589, 2009.

29. **Shweta A, Denton KM, Kett MM, Bertram JF, Lambert GW, Anderson WP.** Paradoxical structural effects in the unilaterally denervated spontaneously hypertensive rat kidney. *J Hypertens* 23: 851–859, 2005.

30. **Tamaki M, Kidoguchi K, Mizobe T, Koyama J, Kondoh T, Sakurai T, Kohmura E, Yokono K, Umetani K.** Carotid artery occlusion and collateral circulation in C57Black/6J mice detected by synchrotron radiation microangiography. *Kobe J Med Sci* 52: 111–118, 2006.

31. **Van Rodijnen WF, Korstjens IJ, Legerstee N, Ter Wee PM, Tangelder GJ.** Direct vasoconstrictor effect of prostaglandin E2 on renal interlobular arteries: role of the EP3 receptor. *Am J Physiol Renal Physiol* 292: F1094–F1101, 2007.

32. **Wang X, Loutzenhiser R.** Determinants of renal microvascular response to ACh: afferent and efferent arteriolar actions of EDHF. *Am J Physiol Renal Physiol* 282: F124–F132, 2002.

33. **Yamamoto T, Tada T, Brodsky SV, Tanaka H, Noiri E, Kajiya F, Goligorsky MS.** Intravital videomicroscopy of peritubular capillaries in renal ischemia. *Am J Physiol Renal Physiol* 282: F1150–F1155, 2002.

34. **Zana F, Klein JC.** A multimodal registration algorithm of eye fundus images using vessels detection and Hough transform. *IEEE Trans Med Imaging* 18: 419–428, 1999.

35. **Zana F, Klein JC.** Segmentation of vessel-like patterns using mathematical morphology and curvature evaluation. *IEEE Trans Image Process* 10: 1010–1019, 2001.